SCIENCE CHINA
Information Sciences

• RESEARCH PAPER •

August 2025, Vol. 68, Iss. 8, 180508:1–180508:12
https://doi.org/10.1007/s11432-025-4470-4

Special Topic: Quantum Information

Third-order exceptional surface in a pseudo-Hermitian superconducting circuit

Guoqiang ZHANG[1*], Siyan LIN[1], Wei FENG[1], Yu WANG[1], Yang YU[2] & Chuiping YANG[1*]

[1]*School of Physics, Hangzhou Normal University, Hangzhou 311121, China*
[2]*School of Physics, Nanjing University, Nanjing 210093, China*

Received 19 January 2025/Revised 29 March 2025/Accepted 3 June 2025/Published online 9 July 2025

Abstract Compared with an isolated exceptional point, exceptional surfaces in non-Hermitian systems are more robust against environment noises, fabrication errors, and experimental uncertainties. Thanks to this, exceptional surfaces can be applied to enhance the sensitivity of sensors and develop new quantum techniques. Over the past few years, several studies have been devoted to studying high-order exceptional surfaces. However, they are restricted to non-Hermitian systems without pseudo-Hermiticity. To date, research on high-order exceptional surfaces in pseudo-Hermitian systems still remains an untouched area. In this work, we propose a pseudo-Hermitian superconducting circuit, which consists of three circularly-coupled superconducting cavities with balanced gain and loss. We then study the third-order exceptional surface in the proposed circuit. By investigating the eigenvalues, we find that in the parameter space, all third-order exceptional points of the circuit form a third-order exceptional line in the parity-time-symmetric case. When the parity-time-symmetric condition is extended to pseudo-Hermitian conditions, we find more third-order exceptional points, which constitute a third-order exceptional surface in the parameter space. The proposed scheme is universal and can be applied to explore third-order exceptional surfaces in other physical systems, such as optomechanical systems, cavity-magnon systems, and photonic micro-ring systems. This work is of fundamental interest in quantum mechanics and opens a way for studying high-order exceptional surfaces in pseudo-Hermitian systems.

Keywords superconducting circuit, exceptional surface, $\mathcal{PT}$ symmetry, pseudo-Hermiticity

Citation Zhang G Q, Lin S Y, Feng W, et al. Third-order exceptional surface in a pseudo-Hermitian superconducting circuit. Sci China Inf Sci, 2025, 68(8): 180508, https://doi.org/10.1007/s11432-025-4470-4

1 Introduction

Over the past decade, a number of studies have been devoted to studying exceptional points (EPs) in non-Hermitian systems [1–23]. The EP refers to the spectral singularity of non-Hermitian Hamiltonians, where both k ($k \geqslant 2$) eigenvalues and eigenstates coalesce [24]. The spectral singularity around EPs can give rise to many intriguing phenomena, such as unidirectional invisibility [25–27], robust wireless power transfer [28,29], asymmetric mode switching [30,31], phonon lasers [32–34], enhancing spontaneous emission [35], and coherent perfect absorption [36–38]. In particular, Quijandría et al. [39] proposed the second-order EP in a superconducting (SC) circuit, and Dogra et al. [40] simulated this on the IBM SC quantum processor. SC circuits are one of promising platforms for implementing quantum information processing and exploring various exotic phenomena (see [41–43] for reviews). In experiments, the second-order EP has been observed in a dissipative SC qubit [44–47] or a coupled system of two dissipative SC resonators [48]. Moreover, Han et al. experimentally characterized the exceptional entanglement transition around a second-order EP [49] and the topological invariant for a third-order EP [50] by measuring the dynamical evolutions of SC circuits.

In many studies, EPs and related applications are associated with the parity-time ($\mathcal{PT}$) symmetry (see, e.g., [51–58]). The $\mathcal{PT}$-symmetric Hamiltonian, satisfying $[H, \mathcal{PT}] = 0$, is a special subset of non-Hermitian Hamiltonians [59]. Usually, the eigenvalues of non-Hermitian Hamiltonians are complex. However, if a non-Hermitian Hamiltonian has the $\mathcal{PT}$ symmetry, it can also possess an entirely real energy spectrum [1–3]. It is worth noting that the $\mathcal{PT}$ symmetry can be extended to the η-pseudo-Hermitian

* Corresponding author (email: zhangguoqiang@hznu.edu.cn, yangcp@hznu.edu.cn)

symmetry [60–62]. Here, η is a Hermitian invertible operator. Different from the $\mathcal{PT}$-symmetric Hamiltonian, the pseudo-Hermitian Hamiltonian is defined by $\eta H \eta^{-1} = H^{\dagger}$, which has the energy-spectrum properties similar to those of the $\mathcal{PT}$-symmetric Hamiltonian. The relationship among non-Hermitian, pseudo-Hermitian, $\mathcal{PT}$-symmetric and Hermitian Hamiltonians is shown in Figure 1(a). In the pseudo-Hermitian case without $\mathcal{PT}$ symmetry, high-order EPs (i.e., kth-order EPs with $k \geqslant 3$) and related applications have been investigated in various physical systems, including cavity-magnon systems [63–65], cavity optomechanical systems [66, 67], multicoil wireless-power-transfer systems [29], radio-frequency circuits [68], and atom-cavity QED systems [69].

Recently, research attention has also shifted to the study of exceptional surfaces (ESs) [70–76]. For a kth-order ES, every point is a kth-order EP. Compared with an isolated EP, ESs have some characteristic properties. ESs are more robust against environment noises, fabrication errors and experimental uncertainties, which enables ES-based sensors to combine sensitivity and robustness [77–80]. In optical systems, the ES can grant substantial mastery over the system's spectral density of states and band structure, with promising avenues for modulating spontaneous emission rates and amplifying nonlinear effects [74]. By engineering ESs via tuning the system parameters, Soleymani et al. [81] observed the chiral perfect absorption with quartic lineshape in a waveguide-coupled microresonator system. In addition, the second-order ES has also been studied for controlling spontaneous emission [82], manipulating direction absorption [83], topological behaviors [84–87], chaotic dynamics [88], and optical amplifiers [89].

Similar to the construction of EPs in various $\mathcal{PT}$- and η-pseudo-Hermitian-symmetric systems, it is critical to combine ESs and $\mathcal{PT}$- and η-pseudo-Hermitian symmetries. Up to now, the second-order ES has been studied in non-Hermitian systems with different symmetries, e.g., $\mathcal{PT}$ symmetry [74], η-pseudo-Hermitian symmetry [75] and parity-particle-hole symmetry [76]. Furthermore, high-order ESs (i.e., kth-order ESs with $k \geqslant 3$) were theoretically proposed [90, 91] and experimentally demonstrated [92]. Specifically, Ref. [92] reported a robust on-chip integrated microlaser source based on ESs, where the performances of the microlaser source can be improved by increasing the order k of ESs. However, these studies (i.e., [90–92]) are restricted to non-Hermitian systems without pseudo-Hermiticity, where the eigenvalues are complex near ESs. In this context, investigating high-order ESs in pseudo-Hermitian systems is highly desirable, as it may offer novel insights into exploring topological properties and related applications of high-order ESs in non-Hermitian areas [74–76].

In this work, we propose a pseudo-Hermitian SC circuit and then study the third-order ES in the circuit. As shown in Figure 1(b), the proposed circuit consists of three SC coplanar waveguide cavities, which are coupled to a common SC qubit. Due to the large detuning between the qubit and the three SC cavities, we can adiabatically eliminate the degrees of freedom of the qubit and obtain an effective non-Hermitian Hamiltonian, which describes three circularly coupled SC cavities mediated by a SC qubit (cf. Subection. 2.1). When the circuit parameters satisfy certain constraints, the circuit possesses the pseudo-Hermiticity, and it has either (i) three real eigenvalues or (ii) one real eigenvalue and two complex-conjugate eigenvalues. In the $\mathcal{PT}$-symmetric case, we find that all third-order EPs of the circuit form a line in the parameter space, i.e., third-order exceptional line (EL). When the $\mathcal{PT}$ symmetry is extended to the η-pseudo-Hermitian symmetry, we find the third-order EL becomes a third-order ES in the parameter space. We further study the energy spectrum of the pseudo-Hermitian SC circuit around third-order EPs. This proposal is universal and can be applied to investigate the third-order ES in other physical systems, such as optomechanical systems [31], cavity-magnon systems [37], and photonic microring systems [52]. This work is of fundamental interest in quantum mechanics [93–95] and opens a way for studying high-order ESs in pseudo-Hermitian systems [63–69].

This paper is organized as follows. In Section 2, we introduce the proposed SC circuit and derive the pseudo-Hermitian conditions for the SC circuit. In Section 3, we investigate the third-order EL of the SC circuit in the $\mathcal{PT}$-symmetric case. In Section 4, we construct the third-order ES of the SC circuit under the pseudo-Hermitian conditions. We end up with brief discussions and conclusion in Section 5.

2 Model

As illustrated in Figure 1(b), the proposed SC circuit consists of three SC coplanar waveguide cavities, which are indirectly coupled via an SC qubit. Below, we first derive the effective Hamiltonian for the three SC cavities by eliminating the degrees of freedom of the qubit in the dispersive regime, and then derive the pseudo-Hermitian conditions for the SC circuit.

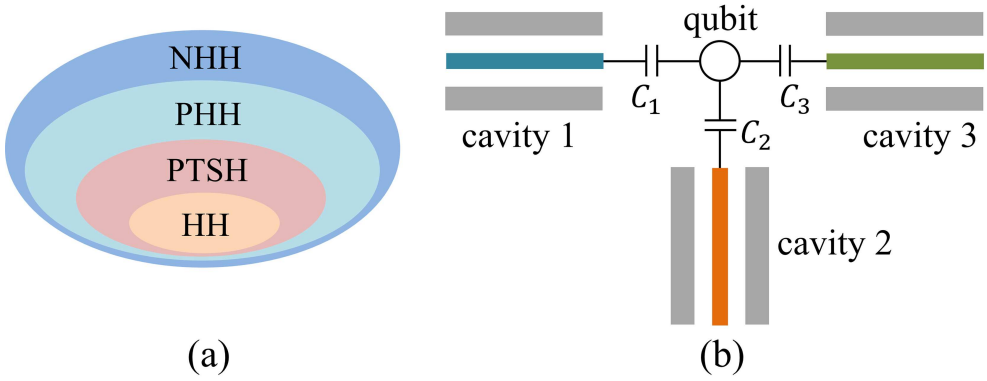

Figure 1 (Color online) (a) The relationship among non-Hermitian, pseudo-Hermitian, $\mathcal{PT}$-symmetric and Hermitian Hamiltonians. In the figure, the non-Hermitian, pseudo-Hermitian, $\mathcal{PT}$-symmetric and Hermitian Hamiltonians are denoted as NHH, PHH, PTSH and HH, respectively. (b) Schematic diagram of the proposed SC circuit, which is composed of three SC coplanar waveguide cavities coupled to an SC qubit (the circle) through capacitances C_1, C_2, and C_3, respectively.

2.1 Effective Hamiltonian of the proposed SC circuit

Consider three SC cavities (labeled as cavity 1, cavity 2, and cavity 3, respectively) coupled to an SC qubit (see Figure 1(b)). The total Hamiltonian of the proposed SC circuit contains two parts:

$$H_{\rm tot} = H_0 + H_{\rm int}. \tag{1}$$

Here, H_0 is the Hamiltonian of bare cavities and qubit given by (hereafter assuming $\hbar = 1$)

$$H_0 = \sum_{n=1}^{3}(\omega_n' - i\kappa_n)a_n^\dagger a_n + (\omega_q - i\gamma)\sigma^+\sigma^-, \tag{2}$$

where a_n and $a_n^\dagger$ $(n = 1, 2, 3)$ are the annihilation and creation operators of cavity n with angular frequency ω_n' and loss rate (or gain rate) κ_n, ω_q is the transition frequency between ground state $|g\rangle$ and excited state $|e\rangle$ of the qubit, γ is the loss rate of the qubit, and $\sigma^- = |g\rangle\langle e|$ and $\sigma^+ = |e\rangle\langle g|$ are the ladder operators of the qubit. In (2), $-i\kappa_n a_n^\dagger a_n$ and $-i\gamma\sigma^+\sigma^-$ describe the dissipations of cavity n and qubit, respectively, which have been widely used in studying EPs [1–5]. Theoretically, this form can be derived using the Langevin equations [66]. If cavity n is passive (active), the loss rate (gain rate) is positive (negative), i.e., $\kappa_n > 0$ ($\kappa_n < 0$). Under the rotating-wave approximation, the interaction Hamiltonian between three cavities and qubit is

$$H_{\rm int} = \sum_{n=1}^{3} g_{nq}(a_n^\dagger\sigma^- + a_n\sigma^+), \tag{3}$$

where g_{nq} $(\geqslant 0)$ is the coupling strength between cavity n and qubit. In our work, we assume that the SC circuit is in the strong-coupling regime, where the circuit parameters satisfy $\{\omega_n', \omega_q\} \gg g_{nq} \gg \{|\kappa_n|, \gamma\}$.

When the frequency detuning of cavity n from the qubit is much larger than the coupling strength g_{nq} between them (i.e., $\omega_n' - \omega_q \gg g_{nq}$, corresponding to the dispersive regime), we can use a Fröhlich-Nakajima transformation $U = \exp(V)$ on the Hamiltonian $H_{\rm tot}$ to decouple the cavities and the qubit [96, 97]. The anti-Hermitian operator V needs to satisfy both $V^\dagger = -V$ and $H_{\rm int} + [H_0, V] \approx 0$. Up to the second order, the transformed Hamiltonian $H_{\rm eff} = U^\dagger H_{\rm tot} U$ can be approximatively expressed as

$$H_{\rm eff} \approx H_0 + \frac{1}{2}[H_I, V]. \tag{4}$$

If we choose

$$V = -\sum_{n=1}^{3}\frac{g_{nq}}{\omega_n' - \omega_q}(a_n^\dagger\sigma^- - a_n\sigma^+), \tag{5}$$

the corresponding effective Hamiltonian is

$$\begin{aligned} H_{\text{eff}} =& \sum_{n=1}^{3}(\omega_n' - i\kappa_n)a_n^\dagger a_n + (\omega_q - i\gamma)\sigma^+\sigma^- \\ &- \sum_{n=1}^{3}\sum_{m>n}^{3} g_{\text{nm}}(a_n^\dagger a_m + a_n a_m^\dagger)\sigma_z \\ &- \sum_{n=1}^{3}\frac{g_{nq}^2}{\omega_n' - \omega_q}(a_n^\dagger a_n\sigma_z + \sigma^+\sigma^-), \end{aligned} \tag{6}$$

where the effective coupling strength g_{nm} between cavity n and cavity m is

$$g_{nm} = \frac{g_{nq}g_{mq}}{2}\left(\frac{1}{\omega_n' - \omega_q} + \frac{1}{\omega_m' - \omega_q}\right). \tag{7}$$

Because the qubit has a large detuning from three SC cavities, we can assume that there is no energy exchange between qubit and cavities. If the SC qubit is initially prepared in its ground state, we can eliminate the degrees of freedom of the qubit by replacing σ_z with -1 in (6). Then, the effective Hamiltonian H_{eff} of three SC cavities can be reduced to

$$H_{\text{eff}} = \sum_{n=1}^{3}(\omega_n - i\kappa_n)a_n^\dagger a_n + \sum_{n=1}^{3}\sum_{m>n}^{3} g_{nm}(a_n^\dagger a_m + a_n a_m^\dagger) \tag{8}$$

with the shifted frequency $\omega_n = \omega_n' + g_{nq}^2/(\omega_n' - \omega_q)$ of cavity n.

The effective Hamiltonian in (8) describes three circularly-coupled SC cavities, which are mediated by the SC qubit. Without loss of generality, we assume that cavity 2 is lossy, i.e.,

$$\kappa_2 > 0. \tag{9}$$

In the absence of cavity 3 (i.e., $g_{13} = g_{23} = 0$), the binary system of cavities 1 and 2 has the $\mathcal{PT}$ symmetry when the system parameters satisfy $\omega_1 = \omega_2$ and $\kappa_1 = -\kappa_2$. This special case has been investigated in [39], where the $\mathcal{PT}$-symmetric phase transition at a second-order EP was studied.

2.2 Pseudo-Hermitian conditions for the SC circuit

In this work, we study the third-order ES of the SC circuit under the pseudo-Hermitian conditions. For the convenience of following calculations, we give the corresponding matrix form H of the non-Hermitian Hamiltonian H_{eff} in (8) via the relation $H_{\text{eff}} = \alpha^\dagger H\alpha$, with $\alpha = (a_1, a_2, a_3)^{\text{T}}$ and

$$H = \begin{pmatrix} \omega_1 - i\kappa_1 & g_{12} & g_{13} \\ g_{12} & \omega_2 - i\kappa_2 & g_{23} \\ g_{13} & g_{23} & \omega_3 - i\kappa_3 \end{pmatrix}. \tag{10}$$

If the SC circuit possesses the pseudo-Hermiticity, the three eigenvalues of the non-Hermitian matrix H are all real or one real and the other two constituting a complex-conjugate pair [60–62]. This energy-spectrum property of the pseudo-Hermitian Hamiltonian is equal to that the non-Hermitian matrix H and its complex-conjugate matrix H^* have the same eigenvalues [63], i.e., $|H - \lambda I| = |H^* - \lambda I| = 0$, where I is an identity matrix and λ is the eigenvalue of the non-Hermitian matrix H. Using the relation $|H - \lambda I| = |H^* - \lambda I|$, we can obtain the pseudo-Hermitian conditions,

$$\begin{aligned} &\kappa_1 + \kappa_2 + \kappa_3 = 0, \\ &\delta_1\kappa_1 + \delta_2\kappa_2 = 0, \\ &g_{12}^2\kappa_3 + g_{13}^2\kappa_2 + g_{23}^2\kappa_1 - \delta_1\delta_2\kappa_3 + \kappa_1\kappa_2\kappa_3 = 0, \end{aligned} \tag{11}$$

where $\delta_{1(2)} = \omega_{1(2)} - \omega_3$ is the frequency detuning of cavity 1 (cavity 2) from cavity 3. Under the pseudo-Hermitian conditions, the characteristic secular equation $|H - \lambda I| = 0$ is reduced to

$$a(\lambda - \omega_3)^3 + b(\lambda - \omega_3)^2 + c(\lambda - \omega_3) + d = 0, \tag{12}$$

where the four coefficients, a, b, c and d, are given by

$$\begin{aligned} a &= 1, \\ b &= -(\delta_1+\delta_2), \\ c &= \delta_1\delta_2-(g_{12}^2+g_{13}^2+g_{23}^2)-(\kappa_1\kappa_2+\kappa_1\kappa_3+\kappa_2\kappa_3), \\ d &= \delta_1 g_{23}^2+\delta_2 g_{13}^2-2g_{12}g_{13}g_{23}+(\delta_1\kappa_2+\delta_2\kappa_1)\kappa_3. \end{aligned} \tag{13}$$

Note that Eq. (12) is a cubic equation for the eigenvalue λ, which has three roots denoted as $\lambda_\pm$ and λ_0. According to the root discriminant of the cubic equation with one unknown [98], the three roots $\lambda_\pm$ and λ_0 are unequally real if the circuit parameters satisfy $\Delta<0$, where

$$\Delta \equiv B^2-4AC \tag{14}$$

is the discriminant, with

$$A=b^2-3ac, \quad B=bc-9ad, \quad C=c^2-3bd. \tag{15}$$

In particular, for $A=B=0$ (satisfying $\Delta=0$), i.e.,

$$\begin{aligned} &(\kappa_1^2+\kappa_1\kappa_2+\kappa_2^2)(\delta_1^2-3\kappa_2^2)+3\kappa_2^2(g_{12}^2+g_{13}^2+g_{23}^2)=0, \\ &(\kappa_1-\kappa_2)\kappa_1\delta_1^3-18\kappa_2^2 g_{13}g_{23}g_{12}+\xi\delta_1\kappa_2=0, \end{aligned} \tag{16}$$

$\lambda_\pm$ and λ_0 coalesce to

$$\lambda_\pm=\lambda_0=\lambda_{\mathrm{EP3}}\equiv\omega_3+\frac{1}{3}(\delta_1+\delta_2), \tag{17}$$

which corresponds to the third-order EP of the SC circuit. The coefficient ξ in (16) is given by

$$\begin{aligned} \xi = {} & (g_{12}^2+9\kappa_1\kappa_2)(\kappa_1-\kappa_2)-g_{13}^2(8\kappa_1+\kappa_2) \\ & +g_{23}^2(\kappa_1+8\kappa_2)+8(\kappa_1^3-\kappa_2^3). \end{aligned} \tag{18}$$

In the other case of $\Delta=0$ but $A\neq0$ and $B\neq0$, only λ_+ and λ_- become coalescent (i.e., $\lambda_+=\lambda_-\neq\lambda_0$), corresponding to the second-order EP of the SC circuit. When $\Delta>0$, only λ_0 is still real, while λ_+ and λ_- form a complex-conjugate pair.

3 Third-order exceptional line in the $\mathcal{PT}$-symmetric case

In the quantum mechanics, the time-reversal operator $\mathcal{T}$ is usually defined by the complex conjugation operator $\mathcal{K}$, i.e., $\mathcal{T}=\mathcal{K}$ [59]. For our system consisting of three SC cavities, the parity operator $\mathcal{P}$ can be represented as

$$\mathcal{P}=\begin{pmatrix} 1 & 0 & 0 \\ 0 & 0 & 1 \\ 0 & 1 & 0 \end{pmatrix}. \tag{19}$$

If the proposed SC circuit owns the $\mathcal{PT}$ symmetry, the matrix form H of the non-Hermitian Hamiltonian given in (10) must satisfy

$$[H,\mathcal{PT}]=0, \tag{20}$$

which is equivalent to $H=\mathcal{PT}H(\mathcal{PT})^{-1}=\mathcal{P}(\mathcal{K}H\mathcal{K}^{-1})\mathcal{P}^{-1}=\mathcal{P}H^*\mathcal{P}^{-1}$. Using the relation $H=\mathcal{P}H^*\mathcal{P}^{-1}$, we obtain the $\mathcal{PT}$-symmetric conditions given by

$$\omega_2=\omega_3, \quad g_{12}=g_{13}, \quad \kappa_1=0, \quad \kappa_3=-\kappa_2. \tag{21}$$

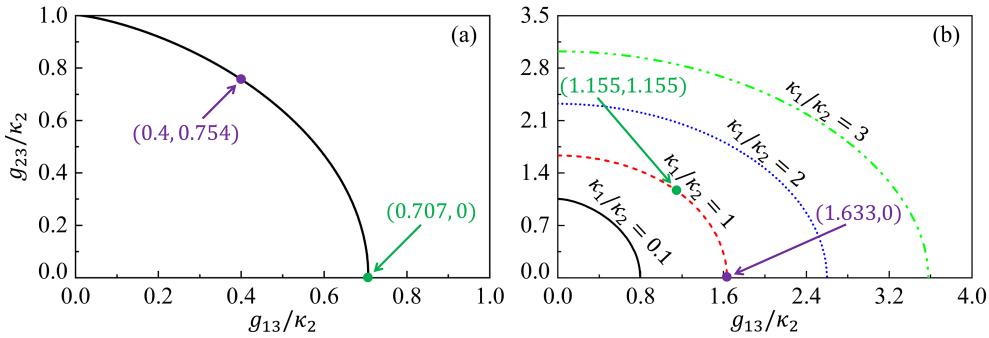

Figure 2 (Color online) (a) Third-order EL in the $\mathcal{PT}$-symmetric case with $\kappa_1 = 0$, obtained by numerically solving (23); (b) third-order ELs for different κ_1/κ_2, obtained by numerically solving (16) under the pseudo-Hermitian conditions in (11). Here $\kappa_1/\kappa_2 = 0.1$ for the (black) solid curve, $\kappa_1/\kappa_2 = 1$ for the (red) dashed curve, $\kappa_1/\kappa_2 = 2$ for the (blue) dotted curve, and $\kappa_1/\kappa_2 = 3$ for the (green) dotted-dashed curve.

It can be easily verified that the $\mathcal{PT}$-symmetric conditions are a special case of the pseudo-Hermitian conditions in (11). With the $\mathcal{PT}$ symmetry, the conditions of third-order EP given in (16) are reduced to

$$\begin{aligned} &\delta_1^2 + 6g_{13}^2 + 3g_{23}^2 - 3\kappa_2^2 = 0, \\ &9g_{23}g_{13}^2 - (4g_{23}^2 - g_{13}^2 - 4\kappa_2^2)\delta_1 = 0. \end{aligned} \tag{22}$$

From the first equation in (22), we have $0 \leqslant g_{13}/\kappa_2 \leqslant 1/\sqrt{2}$ and $0 \leqslant g_{23}/\kappa_2 \leqslant 1$. By eliminating δ_1 in (22), we find the constraint on the coupling strengths g_{13} and g_{23}, given by

$$4g_{23}^2 + 2g_{13}^2 + 3\sqrt[3]{4}g_{13}^{4/3}\kappa_2^{2/3} - 4\kappa_2^2 = 0, \tag{23}$$

which describes a third-order EL, as plotted in Figure 2(a). In the third-order EL, every point corresponds to a third-order EP, where the $\mathcal{PT}$-symmetric phase transition generally occurs [1–3]. For example, at $g_{13}/\kappa_2 = 0.707$ and $g_{23} = 0$ ($g_{13}/\kappa_2 = 0.4$ and $g_{23}/\kappa_2 = 0.754$) indicated by the green dot (purple dot) in Figure 2(a), the corresponding three eigenvalues of the circuit coalesce to $\lambda_\pm = \lambda_0 = \lambda_{\rm EP3} = \omega_3$ ($\lambda_\pm = \lambda_0 = \lambda_{\rm EP3} = \omega_3 - 0.1923\kappa_2$), cf. (17).

Usually, one can observe the EP by measuring the energy spectrum of the system via varying the coupling strength in the experiment, where other system parameters are fixed [1–3]. In the symmetric case of $\omega_1 = \omega_2 = \omega_3$ (i.e., the three cavities are on-resonance), the three eigenvalues $\lambda_\pm$ and λ_0 of the circuit, given by

$$\lambda_\pm = \omega_3 \pm \sqrt{2g_{13}^2 - \kappa_2^2}, \quad \lambda_0 = \omega_3, \tag{24}$$

can be obtained by solving the characteristic equation, i.e., (12), under the $\mathcal{PT}$-symmetric conditions given by (21). According to (24), we find that the SC circuit has three real eigenvalues (one real eigenvalue and two complex-conjugate eigenvalues) in the region $g_{13}/\kappa_2 > 1/\sqrt{2}$ ($g_{13}/\kappa_2 < 1/\sqrt{2}$). This indicates that the circuit is in the $\mathcal{PT}$-symmetric phase for $g_{13}/\kappa_2 > 1/\sqrt{2}$ and the $\mathcal{PT}$-symmetry-breaking phase for $g_{13}/\kappa_2 < 1/\sqrt{2}$, respectively. Particularly, the three eigenvalues coalesce to $\lambda_\pm = \lambda_0 = \lambda_{\rm EP3} = \omega_3$ at $g_{13}/\kappa_2 = 1/\sqrt{2}$, corresponding to the third-order EP indicated by the green dot in Figure 2(a). If we vary the coupling strength g_{13} from $g_{13}/\kappa_2 > 1/\sqrt{2}$ to $g_{13}/\kappa_2 < 1/\sqrt{2}$, the circuit will undergo a phase transition from the $\mathcal{PT}$-symmetric phase to the $\mathcal{PT}$-symmetry-breaking phase at a third-order EP with $g_{13}/\kappa_2 = 1/\sqrt{2}$. In the asymmetric case of $\omega_1 \neq \omega_2 = \omega_3$ (i.e., the three cavities are off-resonance), the third-order EP still exists, but it is difficult to analytically investigate the eigenvalues of the SC circuit because the expressions of three eigenvalues are cumbersome and not shown here.

In Figure 3, we display the energy spectrum of the Hamiltonian $H_{\rm eff}$ in (8) versus the coupling strength g_{13}/κ_2 in the $\mathcal{PT}$-symmetric case. Figures 3(a) and (b) show the real and imaginary parts of the eigenvalues $\lambda_\pm$ and λ_0 given in (24) versus g_{13}/κ_2 in the symmetric case (i.e., $\omega_1 = \omega_2 = \omega_3$). It can be seen that the eigenvalue λ_0 is real for any values of g_{13}/κ_2 (see the solid red curves), while other two eigenvalues λ_+ and λ_- are complex (real) when $g_{13}/\kappa_2 < 0.707$ ($g_{13}/\kappa_2 > 0.707$) (see the dashed black and dotted blue curves). This means that in the region $g_{13}/\kappa_2 > 0.707$ ($g_{13}/\kappa_2 < 0.707$), the circuit is in the

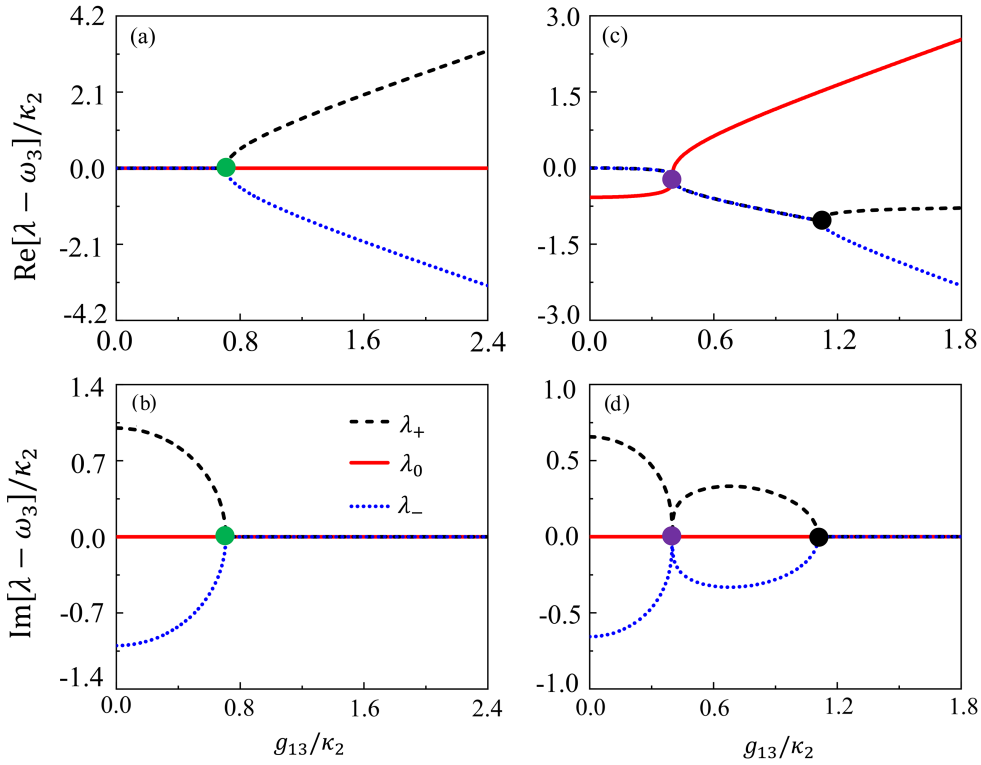

Figure 3 (Color online) Real and imaginary parts of the eigenvalue $(\lambda-\omega_3)/\kappa_2$ as a function of the coupling strength g_{13}/κ_2 in the $\mathcal{PT}$-symmetric case, where the green dots and purple dots indicate third-order EPs, and the black dots indicate second-order EPs. Here $\delta_1=g_{23}=0$ in (a) and (b), while $\delta_1/\kappa_2=-0.5768$ and $g_{23}/\kappa_2=0.7544$ in (c) and (d). Other parameters are $\kappa_1=0$, $\kappa_3/\kappa_2=-1$, $\delta_2=0$, and $g_{12}=g_{13}$.

$\mathcal{PT}$-symmetric phase ($\mathcal{PT}$-symmetry-breaking phase). In particular, for $g_{13}/\kappa_2=0.707$, the three eigenvalues coalesce together (corresponding to a third-order EP), where the $\mathcal{PT}$-symmetric phase transition occurs. Compared with the symmetric case, the eigenvalues of the SC circuit have significantly different characteristics in the asymmetric case (i.e., $\omega_1\neq\omega_2=\omega_3$; cf. Figures 3(a) and (c); Figures 3(b) and (d)), where the results in Figures 3(c) and (d) are obtained by numerically solving the characteristic equation (i.e., (12)) under the $\mathcal{PT}$-symmetric conditions given in (21). As shown in Figures 3(c) and (d), the SC circuit can exhibit a $\mathcal{PT}$-symmetric phase transition at the second-order EP (rather than the third-order EP in the symmetric case; cf. Figures 3(a) and (b)) with $g_{13}/\kappa_2=1.109$, where only two eigenvalues λ_+ and λ_- (see the dashed black and dotted blue curves) are coalescent. In the $\mathcal{PT}$-symmetry-breaking phase with complex eigenvalues, there exists a third-order EP at $g_{13}/\kappa_2=0.401$, marked by the purple dots in Figures 3(c) and (d). Note that no $\mathcal{PT}$-symmetric phase transition occurs at this third-order EP.

4 Third-order exceptional surface under the pseudo-Hermitian conditions

In the last section, we study the third-order EL in the $\mathcal{PT}$-symmetric case. Here we investigate the third-order ES. When $\kappa_1>0$, the SC circuit can own the pseudo-Hermiticity without $\mathcal{PT}$ symmetry. For any given value of κ_1/κ_2 (>0), we can obtain a third-order EL by numerically solving (16) under the pseudo-Hermitian conditions given in (11). In Figure 2(b), we take $\kappa_1/\kappa_2=0.1$, 1, 2, and 3 as an example. At each point in the four third-order ELs, the corresponding three eigenvalues of the SC circuit coalesce to one, such as $\lambda_\pm=\lambda_0=\lambda_{\mathrm{EP3}}=\omega_3$ at $g_{13}/\kappa_2=g_{23}/\kappa_2=1.155$ (indicated by the green dot) and $\lambda_\pm=\lambda_0=\lambda_{\mathrm{EP3}}=\omega_3$ at $g_{13}/\kappa_2=1.633$ and $g_{23}=0$ (indicated by the purple dot). If we continuously vary κ_1/κ_2, these third-order ELs will form a surface in the three-dimensional space (g_{13},g_{23},κ_1). In Figure 4, we plot the distribution of third-order EPs in the space (g_{13},g_{23},κ_1) by numerically solving (16) and (11). These third-order EPs form a third-order ES. Note that the third-order ES also contains the third-order EL in the $\mathcal{PT}$-symmetric case with $\kappa_1=0$, cf. Figure 2(a).

Next, we study the energy spectrum of the SC circuit in the pseudo-Hermitian case with $\kappa_1>0$. For

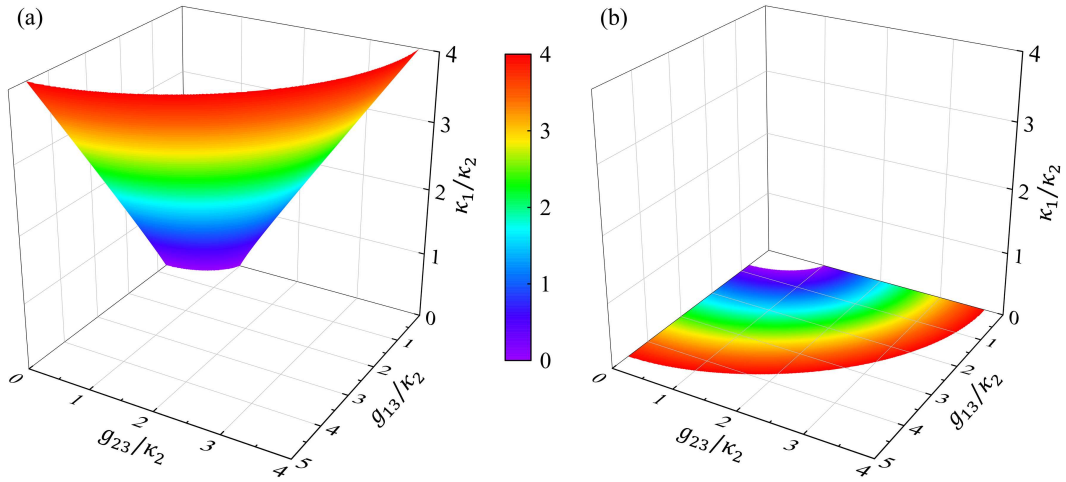

Figure 4 (Color online) (a) Third-order ES obtained by numerically solving (16) under the pseudo-Hermitian conditions in (11); (b) the projection of the third-order ES depicted in (a) in the space of g_{13} and g_{23}. The colors in (a) and (b) represent the values of κ_1/κ_2.

the symmetric case of $\kappa_1/\kappa_2 = 1$, $g_{12} = 0$ and $g_{23} = g_{13}$, the pseudo-Hermitian conditions in (11) are reduced to

$$\kappa_3 = -2\kappa_2, \quad \delta_1 = -\delta_2, \quad \delta_2 = \sqrt{g_{13}^2 - \kappa_2^2}. \tag{25}$$

The third equation in (25) means that there is the pseudo-Hermiticity for the circuit only when the coupling strength g_{13} satisfies $g_{13}^2 - \kappa_2^2 \geqslant 0$, i.e., $g_{13}/\kappa_2 \geqslant 1$. This feature is significantly different from the $\mathcal{PT}$-symmetric case, where the SC circuit has the $\mathcal{PT}$ symmetry for any value of g_{13} (cf. (21) and related discussions). Under the pseudo-Hermitian conditions given in (25), the three eigenvalues of the SC circuit are given by

$$\lambda_\pm = \omega_3 \pm \sqrt{3g_{13}^2 - 4\kappa_2^2}, \quad \lambda_0 = \omega_3. \tag{26}$$

In the region $g_{13}/\kappa_2 > 2/\sqrt{3}$, the SC circuit has three real eigenvalues. For $g_{13}/\kappa_2 = 2/\sqrt{3}$ in particular, the three eigenvalues $\lambda_\pm$ and λ_0 coalesce to $\lambda_\pm = \lambda_0 = \lambda_{\rm EP3} = \omega_3$, corresponding to the third-order EP indicated by the green dot in Figure 2(b). While, for $1 \leqslant g_{13}/\kappa_2 < 2/\sqrt{3}$, λ_0 is also real but λ_+ and λ_- become complex. In addition, we take an asymmetric case with $\kappa_1/\kappa_2 = 1$, $g_{12} = g_{13}/\sqrt{8}$ and $g_{23} = 0$. Now the pseudo-Hermitian conditions in (11) become

$$\kappa_3 = -2\kappa_2, \quad \delta_1 = -\delta_2, \quad \delta_2 = \sqrt{3g_{13}^2/8 - \kappa_2^2}, \tag{27}$$

which indicates that the allowed minimal value of the coupling strength g_{13} is $g_{13} = \sqrt{8/3}\kappa_2$ to ensure $3g_{13}^2/8 - \kappa_2^2 \geqslant 0$. In this circumstance, we do not show the cumbersome expressions of three eigenvalues and only give the coalesced eigenvalues $\lambda_\pm = \lambda_0 = \lambda_{\rm EP3} = \omega_3$ at $g_{13}/\kappa_2 = \sqrt{8/3}$, indicated by the purple dot in Figure 2(b).

Furthermore, we plot the energy spectrum of the pseudo-Hermitian SC circuit without $\mathcal{PT}$ symmetry in Figure 5. Note that in the yellow regions, no pseudo-Hermiticity exists. Figures 5(a) and (b) display the real and imaginary parts of the eigenvalues $\lambda_\pm$ and λ_0, given in (26), as a function of the coupling strength g_{13}/κ_2 for the symmetric case of $\kappa_1/\kappa_2 = 1$, $g_{12} = 0$ and $g_{23} = g_{13}$. In the region $1 \leqslant g_{13}/\kappa_2 < 1.155$, the pseudo-Hermitian circuit has one real eigenvalue (see the solid red curves) and two complex-conjugate eigenvalues (see the dashed black and dotted blue curves). At the critical coupling strength $g_{13}/\kappa_2 = 1.155$, the three eigenvalues $\lambda_\pm$ and λ_0 coalesce to $\lambda_\pm = \lambda_0 = \lambda_{\rm EP3} = \omega_3$, which is a third-order EP of the pseudo-Hermitian circuit. When $g_{13}/\kappa_2 > 1.155$, all three eigenvalues are real. In the asymmetric case of $\kappa_1/\kappa_2 = 1$, $g_{12} = g_{13}/\sqrt{8}$ and $g_{23} = 0$, the real and imaginary parts of the eigenvalues $\lambda_\pm$ and λ_0, obtained by numerically solving (12) under the pseudo-Hermitian conditions in (27), are also shown in Figures 5(c) and (d), where the eigenvalues exist in the region $g_{13}/\kappa_2 \geqslant 1.633$. In addition to the third-order EP at $g_{13}/\kappa_2 = 1.633$ (corresponding to $\lambda_\pm = \lambda_0 = \lambda_{\rm EP3} = \omega_3$), the eigenvalue λ_0 is real (see

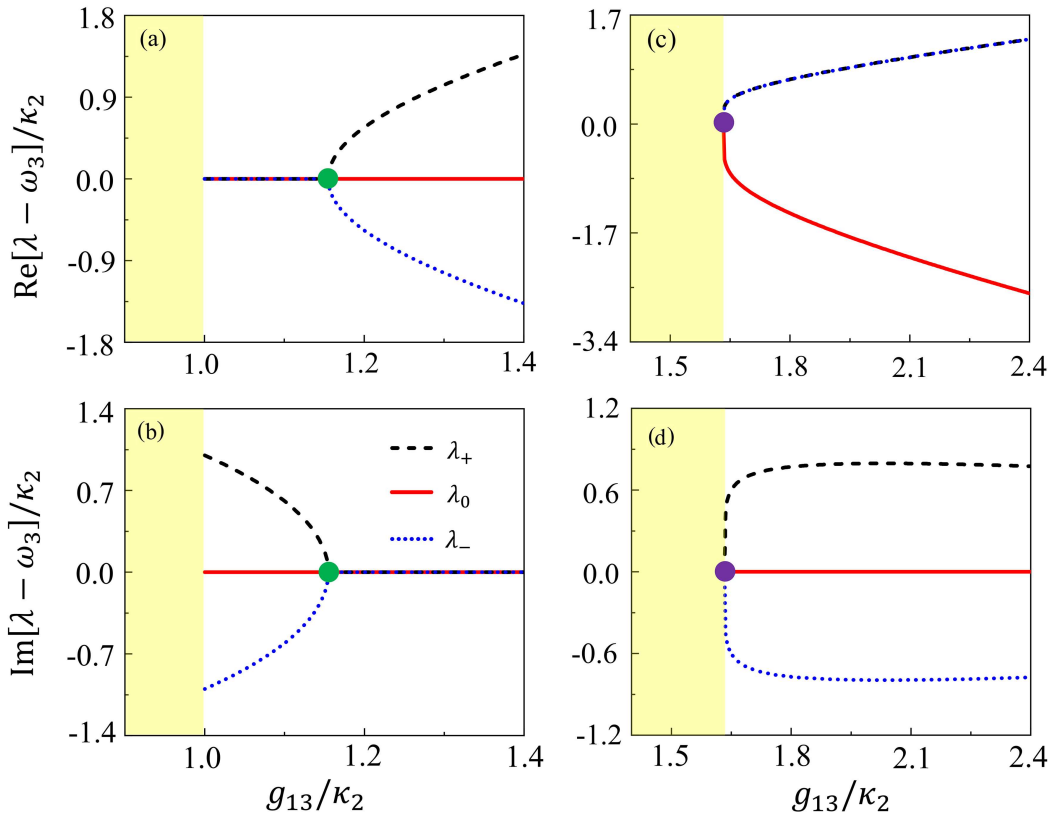

Figure 5 (Color online) Real and imaginary parts of the eigenvalue $(\lambda-\omega_3)/\kappa_2$ versus the coupling strength g_{13}/κ_2 in the pseudo-Hermitian case without $\mathcal{PT}$ symmetry, where the green dots and purple dots indicate third-order EPs. Note that in the yellow regions, the SC circuit does not have the pseudo-Hermiticity. Here $g_{12}=0$, $g_{23}=g_{13}$ and $\delta_2=\sqrt{g_{13}^2-\kappa_2^2}$ in (a) and (b), while $g_{12}=g_{13}/\sqrt{8}$, $g_{23}=0$ and $\delta_2=\sqrt{3g_{13}^2/8-\kappa_2^2}$ in (c) and (d). Other parameters are $\kappa_1/\kappa_2=1$, $\kappa_3/\kappa_2=-2$ and $\delta_1=-\delta_2$.

the solid red curves) while the eigenvalues λ_+ and λ_- are complex-conjugate (see the dashed black and dotted blue curves) for any allowed values of g_{13}. Different from Figure 3, there are no second-order EPs in Figure 5. This discrepancy is primarily attributed to the parameter selection. By carefully choosing appropriate parameters, second-order EPs can also emerge even in the pseudo-Hermitian case without $\mathcal{PT}$ symmetry (see, e.g., [66]). A thorough investigation of this topic is beyond the scope of the current study and is not shown here.

5 Discussions and conclusion

If more SC cavities are coupled to an SC qubit, higher-order ESs, such as fourth-order and fifth-order ESs, can also be constructed using a similar methodology outlined in the paper. As the order of ESs increases, the complexity of the construction process will grow significantly. By introducing additional symmetries into the pseudo-Hermitian circuit, it is expected to effectively reduce the complexity [75,76]. On the other hand, the Liouvillian EP has garnered extensive attention in research, which is defined via the degeneracy of a Liouvillian superoperator [99–101]. This is very different from the Hamiltonian EP, with the degeneracy of a non-Hermitian Hamiltonian. However, existing studies exclusively focused on ESs consisting of Hamiltonian EPs [70–92]. In the future, it is a fascinating topic to explore the Liouvillian ES, on which each point is a Liouvillian EP. The Liouville spectrum is relatively complex, which gives rise to the challenge in constructing Liouvillian ESs. One potential approach to addressing this challenge is to incorporate symmetries into the Liouvillian superoperator [75,76].

Previous studies have primarily focused on high-order ESs without pseudo-Hermiticity [90–92]. This paper presents the first study of the high-order ES in a pseudo-Hermitian circuit. The pseudo-Hermitian nature of the circuit ensures that all eigenvalues on the third-order ES are real. In the parameter space, certain EPs on the third-order ES mark the boundaries of the phase transition between η-pseudo-

Hermiticity broken and unbroken regions (with complex eigenvalues and real eigenvalues, respectively). In addition, non-Hermitian systems serve as an excellent platform for exploring diverse symmetries. The study of second-order ESs and their topological properties has been actively conducted in non-Hermitian systems with different symmetries, such as $\mathcal{PT}$ symmetry [74], η-pseudo-Hermitian symmetry [75] and parity-particle-hole symmetry [76]. Combining high-order ESs with pseudo-Hermiticity holds significant promise for uncovering their topological properties and potential applications. For instance, the third-order ES with pseudo-Hermiticity may further improve the performance of ES-based sensors, as the pseudo-Hermiticity can effectively narrow the spectral linewidths of non-Hermitian systems, and EPs on high-order ESs are more sensitive to weak external perturbations [52, 64].

Before concluding, we briefly discuss the experimental feasibility of the proposal in SC circuits. In experiments, the typical frequency for an SC cavity can be made as 1–10 GHz, and the loss rate of an SC cavity is on the order of 0.1–1 MHz [102]. By embedding an SC quantum interference device (SQUID) in an SC cavity, the frequency of the SC cavity can be readily tunable via controlling the bias magnetic flux threading the SQUID loop [48]. As for the active SC cavity, its gain rate can be adjusted (ranging from 0 to 6 MHz) via controlling the drive field on the auxiliary SC qubit, which is transversely coupled to the SC cavity [39, 103]. In addition, the coupling strength between SC cavities can be tuned by varying the cavity-qubit coupling strength [104, 105]. With these accessible technologies, our proposal is experimentally feasible.

In summary, we have studied the third-order ES in the proposed pseudo-Hermitian SC circuit composed of three circularly-coupled SC cavities, where the gain and loss are balanced. Using the energy-spectrum properties of the pseudo-Hermitian Hamiltonian, we have derived the pseudo-Hermitian conditions for the SC circuit. For the $\mathcal{PT}$-symmetric case, we found that all third-order EPs of the circuit are located on a third-order EL in the parameter space. By investigating the eigenvalues of the circuit versus the coupling strength, we have discovered that the circuit exhibits the $\mathcal{PT}$-symmetric phase transition at a third-order EP. Under the pseudo-Hermitian conditions, we found that all third-order EPs form a third-order ES in the parameter space, which contains the third-order EL in the $\mathcal{PT}$-symmetric case. In the pseudo-Hermitian case without $\mathcal{PT}$ symmetry, we have also studied the energy spectrum of the SC circuit around third-order EPs. To the best of our knowledge, this work is the first to study high-order ESs in pseudo-Hermitian systems. These results are of fundamental interest, which may be found in applications in enhancing the sensitivity of sensors and developing new quantum techniques.

Acknowledgements This work was supported by National Natural Science Foundation of China (Grant Nos. U21A20436, 12205069, 12204139, 12404404) and National Key Research and Development Program of China (Grant No. 2024YFA1408900).

References

1 Feng L, El-Ganainy R, Ge L. Non-Hermitian photonics based on parity-time symmetry. Nat Photon, 2017, 11: 752–762
2 El-Ganainy R, Makris K G, Khajavikhan M, et al. Non-Hermitian physics and $\mathcal{PT}$ symmetry. Nat Phys, 2018, 14: 11–19
3 Özdemir Ş K, Rotter S, Nori F, et al. Parity-time symmetry and exceptional points in photonics. Nat Mater, 2019, 18: 783–798
4 Wiersig J. Review of exceptional point-based sensors. Photon Res, 2020, 8: 1457–1467
5 Bergholtz E J, Budich J C, Kunst F K. Exceptional topology of non-Hermitian systems. Rev Mod Phys, 2021, 93: 015005
6 Longhi S, Feng L. Unidirectional lasing in semiconductor microring lasers at an exceptional point. Photon Res, 2017, 5: B1
7 Zhou H, Peng C, Yoon Y, et al. Observation of bulk Fermi arc and polarization half charge from paired exceptional points. Science, 2018, 359: 1009–1012
8 Yang B, Guo Q, Tremain B, et al. Ideal Weyl points and helicoid surface states in artificial photonic crystal structures. Science, 2018, 359: 1013–1016
9 Huang R, Özdemir Ş K, Liao J, et al. Exceptional photon blockade: engineering photon blockade with chiral exceptional points. Laser Photonics Rev, 2022, 16: 2100430
10 Jin L. Parity-time-symmetric coupled asymmetric dimers. Phys Rev A, 2018, 97: 012121
11 Wiersig J. Enhancing the sensitivity of frequency and energy splitting detection by using exceptional points: application to microcavity sensors for single-particle detection. Phys Rev Lett, 2014, 112: 203901
12 Chen W, Kaya Özdemir Ş, Zhao G, et al. Exceptional points enhance sensing in an optical microcavity. Nature, 2017, 548: 192–196
13 Minganti F, Huybrechts D, Elouard C, et al. Creating and controlling exceptional points of non-Hermitian hamiltonians via homodyne Lindbladian invariance. Phys Rev A, 2022, 106: 042210
14 Zhang G Q, Chen Z, Xu D, et al. Exceptional point and cross-relaxation effect in a hybrid quantum system. PRX Quantum, 2021, 2: 020307
15 Song P, Ruan X, Ding H, et al. Experimental realization of on-chip few-photon control around exceptional points. Nat Commun, 2024, 15: 9848
16 Wang C, Jiang X, Zhao G, et al. Electromagnetically induced transparency at a chiral exceptional point. Nat Phys, 2020, 16: 334–340
17 Minganti F, Arkhipov I I, Miranowicz A, et al. Liouvillian spectral collapse in the Scully-Lamb laser model. Phys Rev Res, 2021, 3: 043197
18 Wang B, Liu Z X, Kong C, et al. Mechanical exceptional-point-induced transparency and slow light. Opt Express, 2019, 27: 8069–8080
19 Lu T X, Zhang H, Zhang Q, et al. Exceptional-point-engineered cavity magnomechanics. Phys Rev A, 2021, 103: 063708
20 Lin J D, Kuo P C, Lambert N, et al. Non-Markovian quantum exceptional points. Nat Commun, 2025, 16: 1289

21 Zhang J W, Zhang J Q, Ding G Y, et al. Dynamical control of quantum heat engines using exceptional points. Nat Commun, 2022, 13: 6225
22 Li Z Z, Chen W, Abbasi M, et al. Speeding up entanglement generation by proximity to higher-order exceptional points. Phys Rev Lett, 2023, 131: 100202
23 Arkhipov I I, Minganti F, Miranowicz A, et al. Restoring adiabatic state transfer in time-modulated non-Hermitian systems. Phys Rev Lett, 2024, 133: 113802
24 Heiss W D. The physics of exceptional points. J Phys A-Math Theor, 2012, 45: 444016
25 Lin Z, Ramezani H, Eichelkraut T, et al. Unidirectional invisibility induced by $\mathcal{PT}$-symmetric periodic structures. Phys Rev Lett, 2011, 106: 213901
26 Peng B, Özdemir Ş K, Lei F, et al. Parity-time-symmetric whispering-gallery microcavities. Nat Phys, 2014, 10: 394–398
27 Chatzidimitriou D, Pitilakis A, Yioultsis T, et al. Breaking reciprocity in a non-Hermitian photonic coupler with saturable absorption. Phys Rev A, 2021, 103: 053503
28 Assawaworrarit S, Yu X, Fan S. Robust wireless power transfer using a nonlinear parity-time-symmetric circuit. Nature, 2017, 546: 387–390
29 Hao X, Yin K, Zou J, et al. Frequency-stable robust wireless power transfer based on high-order pseudo-Hermitian physics. Phys Rev Lett, 2023, 130: 077202
30 Doppler J, Mailybaev A A, Böhm J, et al. Dynamically encircling an exceptional point for asymmetric mode switching. Nature, 2016, 537: 76–79
31 Xu H, Mason D, Jiang L, et al. Topological energy transfer in an optomechanical system with exceptional points. Nature, 2016, 537: 80–83
32 Jing H, Özdemir S K, Lü X Y, et al. $\mathcal{PT}$-symmetric phonon laser. Phys Rev Lett, 2014, 113: 053604
33 Zhang J, Peng B, Özdemir Ş K, et al. A phonon laser operating at an exceptional point. Nat Photon, 2018, 12: 479–484
34 Lü H, Özdemir S K, Kuang L M, et al. Exceptional points in random-defect phonon lasers. Phys Rev Appl, 2017, 8: 044020
35 Lin Z, Pick A, Lončar M, et al. Enhanced spontaneous emission at third-order Dirac exceptional points in inverse-designed photonic crystals. Phys Rev Lett, 2016, 117: 107402
36 Sun Y, Tan W, Li H, et al. Experimental demonstration of a coherent perfect absorber with PT phase transition. Phys Rev Lett, 2014, 112: 143903
37 Zhang D, Luo X Q, Wang Y P, et al. Observation of the exceptional point in cavity magnon-polaritons. Nat Commun, 2017, 8: 1368
38 Wang C, Sweeney W R, Stone A D, et al. Coherent perfect absorption at an exceptional point. Science, 2021, 373: 1261–1265
39 Quijandría F, Naether U, Özdemir S K, et al. $\mathcal{PT}$-symmetric circuit QED. Phys Rev A, 2018, 97: 053846
40 Dogra S, Melnikov A A, Paraoanu G S. Quantum simulation of parity-time symmetry breaking with a superconducting quantum processor. Commun Phys, 2021, 4: 26
41 Xiang Z L, Ashhab S, You J Q, et al. Hybrid quantum circuits: superconducting circuits interacting with other quantum systems. Rev Mod Phys, 2013, 85: 623–653
42 Schoelkopf R J, Girvin S M. Wiring up quantum systems. Nature, 2008, 451: 664–669
43 Kurizki G, Bertet P, Kubo Y, et al. Quantum technologies with hybrid systems. Proc Natl Acad Sci USA, 2015, 112: 3866–3873
44 Naghiloo M, Abbasi M, Joglekar Y N, et al. Quantum state tomography across the exceptional point in a single dissipative qubit. Nat Phys, 2019, 15: 1232–1236
45 Chen W, Abbasi M, Joglekar Y N, et al. Quantum jumps in the non-Hermitian dynamics of a superconducting qubit. Phys Rev Lett, 2021, 127: 140504
46 Chen W, Abbasi M, Ha B, et al. Decoherence-induced exceptional points in a dissipative superconducting qubit. Phys Rev Lett, 2022, 128: 110402
47 Wang Z, Xiang Z, Liu T, et al. Observation of the exceptional point in superconducting qubit with dissipation controlled by parametric modulation. Chin Phys B, 2021, 30: 100309
48 Partanen M, Goetz J, Tan K Y, et al. Exceptional points in tunable superconducting resonators. Phys Rev B, 2019, 100: 134505
49 Han P R, Wu F, Huang X J, et al. Exceptional entanglement phenomena: non-Hermiticity meeting nonclassicality. Phys Rev Lett, 2023, 131: 260201
50 Han P R, Ning W, Huang X J, et al. Measuring topological invariants for higher-order exceptional points in quantum three-mode systems. Nat Commun, 2024, 15: 10293
51 Liu Z P, Zhang J, Özdemir Ş K, et al. Metrology with $\mathcal{PT}$-symmetric cavities: enhanced sensitivity near the $\mathcal{PT}$-phase transition. Phys Rev Lett, 2016, 117: 110802
52 Hodaei H, Hassan A U, Wittek S, et al. Enhanced sensitivity at higher-order exceptional points. Nature, 2017, 548: 187–191
53 Feng L, Wong Z J, Ma R M, et al. Single-mode laser by parity-time symmetry breaking. Science, 2014, 346: 972–975
54 Zhang J, Peng B, Özdemir Ş K, et al. Giant nonlinearity via breaking parity-time symmetry: a route to low-threshold phonon diodes. Phys Rev B, 2015, 92: 115407
55 Arkhipov I I, Miranowicz A, Minganti F, et al. Dynamically crossing diabolic points while encircling exceptional curves: a programmable symmetric-asymmetric multimode switch. Nat Commun, 2023, 14: 2076
56 Chen D X, Zhang Y, Zhao J L, et al. Quantum state discrimination in a $\mathcal{PT}$-symmetric system. Phys Rev A, 2022, 106: 022438
57 Xu H, Lai D G, Qian Y B, et al. Optomechanical dynamics in the $\mathcal{PT}$- and broken-$\mathcal{PT}$-symmetric regimes. Phys Rev A, 2021, 104: 053518
58 Hodaei H, Miri M A, Heinrich M, et al. Parity-time-symmetric microring lasers. Science, 2014, 346: 975–978
59 Bender C M, Boettcher S. Real spectra in non-Hermitian Hamiltonians having $\mathcal{PT}$ symmetry. Phys Rev Lett, 1998, 80: 5243–5246
60 Mostafazadeh A. Pseudo-Hermiticity versus $\mathcal{PT}$ symmetry: the necessary condition for the reality of the spectrum of a non-Hermitian Hamiltonian. J Math Phys, 2002, 43: 205–214
61 Mostafazadeh A. Pseudo-Hermiticity versus $\mathcal{PT}$-symmetry. II. A complete characterization of non-Hermitian Hamiltonians with a real spectrum. J Math Phys, 2002, 43: 2814–2816
62 Mostafazadeh A. Pseudo-Hermiticity versus $\mathcal{PT}$-symmetry III: equivalence of pseudo-Hermiticity and the presence of anti-linear symmetries. J Math Phys, 2002, 43: 3944–3951
63 Zhang G Q, You J Q. Higher-order exceptional point in a cavity magnonics system. Phys Rev B, 2019, 99: 054404
64 Zhang G Q, Wang Y, Xiong W. Detection sensitivity enhancement of magnon Kerr nonlinearity in cavity magnonics induced by coherent perfect absorption. Phys Rev B, 2023, 107: 064417
65 Hu Y D, Wang Y P, Shen R C, et al. Synthetically enhanced sensitivity using higher-order exceptional point and coherent perfect absorption. 2024. ArXiv:2401.01613
66 Xiong W, Li Z, Song Y, et al. Higher-order exceptional point in a pseudo-Hermitian cavity optomechanical system. Phys Rev A, 2021, 104: 063508
67 Xiong W, Li Z, Zhang G Q, et al. Higher-order exceptional point in a blue-detuned non-Hermitian cavity optomechanical

system. Phys Rev A, 2022, 106: 033518
68 Yin K, Hao X, Huang Y, et al. High-order exceptional points in pseudo-Hermitian radio-frequency circuits. Phys Rev Appl, 2023, 20: L021003
69 Li Z, Li X, Zhang G, et al. Realizing strong photon blockade at exceptional points in the weak coupling regime. Front Phys, 2023, 11: 1168372
70 Zhong Q, Ren J, Khajavikhan M, et al. Sensing with exceptional surfaces in order to combine sensitivity with robustness. Phys Rev Lett, 2019, 122: 153902
71 Budich J C, Carlström J, Kunst F K, et al. Symmetry-protected nodal phases in non-Hermitian systems. Phys Rev B, 2019, 99: 041406
72 Zhang X, Ding K, Zhou X, et al. Experimental observation of an exceptional surface in synthetic dimensions with magnon polaritons. Phys Rev Lett, 2019, 123: 237202
73 Qin G, Xie R, Zhang H, et al. Experimental realization of sensitivity enhancement and suppression with exceptional surfaces. Laser Photonics Rev, 2021, 15: 2000569
74 Zhou H, Lee J Y, Liu S, et al. Exceptional surfaces in $\mathcal{PT}$-symmetric non-Hermitian photonic systems. Optica, 2019, 6: 190–193
75 Grigoryan V L, Xia K. Pseudo-Hermitian magnon-polariton system with a three-dimensional exceptional surface. Phys Rev B, 2022, 106: 014404
76 Okugawa R, Yokoyama T. Topological exceptional surfaces in non-Hermitian systems with parity-time and parity-particle-hole symmetries. Phys Rev B, 2019, 99: 041202
77 Li W, Zhou Y, Han P, et al. Exceptional-surface-enhanced rotation sensing with robustness in a whispering-gallery-mode microresonator. Phys Rev A, 2021, 104: 033505
78 de Carlo M, de Leonardis F, Soref R A, et al. Design of an exceptional-surface-enhanced silicon-on-insulator optical accelerometer. J Lightwave Technol, 2021, 39: 5954–5961
79 de Carlo M, de Leonardis F, Soref R A, et al. Design of a trap-assisted exceptional-surface-enhanced silicon-on-insulator particle sensor. J Lightwave Technol, 2022, 40: 6021–6029
80 Jiang S, Li J, Li Z, et al. Experimental realization of exceptional surfaces enhanced displacement sensing with robustness. Appl Phys Lett, 2023, 123: 201106
81 Soleymani S, Zhong Q, Mokim M, et al. Chiral and degenerate perfect absorption on exceptional surfaces. Nat Commun, 2022, 13: 599
82 Zhong Q, Hashemi A, Özdemir Ş K, et al. Control of spontaneous emission dynamics in microcavities with chiral exceptional surfaces. Phys Rev Res, 2021, 3: 013220
83 Zhong Q, Nelson S, Özdemir Ş K, et al. Controlling directional absorption with chiral exceptional surfaces. Opt Lett, 2019, 44: 5242
84 Tang W, Ding K, Ma G. Realization and topological properties of third-order exceptional lines embedded in exceptional surfaces. Nat Commun, 2023, 14: 6660
85 Jia H, Zhang R Y, Hu J, et al. Topological classification for intersection singularities of exceptional surfaces in pseudo-Hermitian systems. Commun Phys, 2023, 6: 293
86 Stålhammar M, Bergholtz E J. Classification of exceptional nodal topologies protected by $\mathcal{PT}$ symmetry. Phys Rev B, 2021, 104: L201104
87 Wang P, Jin L, Song Z. Berry curvature inside a $\mathcal{PT}$-symmetry protected exceptional surface. Phys Rev B, 2024, 109: 115406
88 Chen L, Wu W, Huang F, et al. Chaotic dynamics on exceptional surfaces. Phys Rev A, 2022, 105: L031501
89 Zhong Q, Ozdemir S K, Eisfeld A, et al. Exceptional-point-based optical amplifiers. Phys Rev Appl, 2020, 13: 014070
90 Yang H, Mao X, Qin G Q, et al. Scalable higher-order exceptional surface with passive resonators. Opt Lett, 2021, 46: 4025–4028
91 Zhang C, Cheng Y, Wang S. Light funneling by spin-orbit-coupled chiral particles on an arbitrary order exceptional surface. Opt Express, 2022, 30: 42495–42503
92 Liao K, Zhong Y, Du Z, et al. On-chip integrated exceptional surface microlaser. Sci Adv, 2023, 9: eadf3470
93 Li N C, Xu L, Liu J M. Experimental realization of deterministic joint remote preparation of an arbitrary two-qubit pure state via GHZ states. Sci China Inf Sci, 2024, 67: 139402
94 Ren S Y, Han D M, Wang M H, et al. Continuous variable quantum teleportation and remote state preparation between two space-separated local networks. Sci China Inf Sci, 2024, 67: 142502
95 Lu Q H, Wang F X, Chen W, et al. Quantum key distribution over a mimicked dynamic-scattering channel. Sci China Inf Sci, 2024, 67: 142503
96 Fröhlich H. Theory of the superconducting state. I. The ground state at the absolute zero of temperature. Phys Rev, 1950, 79: 845–856
97 Nakajima S. Perturbation theory in statistical mechanics. Adv Phys, 1955, 4: 363–380
98 Korn G A, Korn T M. Mathematical Handbook for Scientists and Engineers. New York: McGraw-Hill, 1968
99 Minganti F, Miranowicz A, Chhajlany R W, et al. Quantum exceptional points of non-Hermitian Hamiltonians and Liouvillians: the effects of quantum jumps. Phys Rev A, 2019, 100: 062131
100 Minganti F, Miranowicz A, Chhajlany R W, et al. Hybrid-liouvillian formalism connecting exceptional points of non-Hermitian Hamiltonians and Liouvillians via postselection of quantum trajectories. Phys Rev A, 2020, 101: 062112
101 Arkhipov I I, Miranowicz A, Minganti F, et al. Liouvillian exceptional points of any order in dissipative linear bosonic systems: coherence functions and switching between $\mathcal{PT}$ and anti-$\mathcal{PT}$ symmetries. Phys Rev A, 2020, 102: 033715
102 Gu X, Kockum A F, Miranowicz A, et al. Microwave photonics with superconducting quantum circuits. Phys Rep, 2017, 718-719: 1–102
103 Zhang G Q, Chen Z, You J Q. Experimentally accessible quantum phase transition in a non-Hermitian Tavis-Cummings model engineered with two drive fields. Phys Rev A, 2020, 102: 032202
104 Hoffman A J, Srinivasan S J, Gambetta J M, et al. Coherent control of a superconducting qubit with dynamically tunable qubit-cavity coupling. Phys Rev B, 2011, 84: 184515
105 Whittaker J D, da Silva F C S, Allman M S, et al. Tunable-cavity QED with phase qubits. Phys Rev B, 2014, 90: 024513